Deviation from Gaussianity in the cosmic microwave background temperature fluctuations

Armando Bernui[1], Constantino Tsallis[2] and Thyrso Villela[1]

[1] *Instituto Nacional de Pesquisas Espaciais, Divisão de Astrofísica - Av. dos Astronautas 1758,*
12227-010 São José dos Campos, SP, Brazil
[2] *Centro Brasileiro de Pesquisas Físicas - Rua Xavier Sigaud 150, 22290-180 Rio de Janeiro, RJ, Brazil*

Abstract – Recent measurements of the temperature fluctuations of the cosmic microwave background (CMB) radiation from the WMAP satellite provide indication of a non-Gaussian behavior. Although the observed feature is small, it is detectable and analyzable. Indeed, the temperature distribution $P^{\mathrm{CMB}}(\Delta T)$ of these data can be quite well fitted by the anomalous probability distribution emerging within nonextensive statistical mechanics, based on the entropy $S_q \equiv k\{1 - \int \mathrm{d}x\,[P(x)]^q\}/(q-1)$ $(S_1 = -k \int \mathrm{d}x\,P(x)\ln[P(x)])$. For the CMB frequencies analysed, $\nu = 40.7$, 60.8, and 93.5 GHz, $P^{\mathrm{CMB}}(\Delta T)$ is well described by $P_q(\Delta T) \propto 1/[1 + (q-1)B(\nu)(\Delta T)^2]^{1/(q-1)}$, with $q = 1.04 \pm 0.01$, the strongest non-Gaussian contribution coming from the South-East sector of the celestial sphere. Moreover, Monte Carlo simulations exclude, at the 99% confidence level, $P_1(\Delta T) \propto e^{-B(\nu)(\Delta T)^2}$ to fit the three-year data.

Statistical properties of the CMB **temperature fluctuations.** – Since the early '90s a set of precise observations showed that the angular distribution of the cosmic microwave background (CMB) radiation presents tiny fluctuations, of the order of 10^{-5}, around the equilibrium temperature T_0. These CMB temperature fluctuations, denoted $\Delta T(\theta, \phi)$, are functions of the direction of observation in the celestial sphere (θ, ϕ) and can be expressed by using a spherical harmonic expansion $\Delta T(\theta, \phi)/T_0 = \sum_{\ell m} a_{\ell m} Y_{\ell m}(\theta, \phi)$. Standard cosmological theory predicts that the complex $a_{\ell m}$ modes are statistically isotropic and Gaussian random fields of zero mean ($\langle a_{\ell m} \rangle = 0$) and non-zero variance ($\langle a_{\ell' m'}^* a_{\ell m} \rangle \neq 0$). The fact that ΔT is a real quantity yields consistency relationships between the real and imaginary parts of $a_{\ell m}$ and $a_{\ell - m}$. *Gaussian randomness* means that both real and imaginary parts of the $a_{\ell m}$ are each an independent random variable obeying a Gaussian distribution of zero mean. *Statistical isotropy* means that the variance, which in principle could be different for each ℓ and m, depends only on ℓ, *i.e.* $\langle a_{\ell' m'}^* a_{\ell m} \rangle = \mathcal{C}_\ell\, \delta_{\ell' \ell}\, \delta_{m' m}$. Thus, in the standard inflationary big-bang model, one expects that the CMB temperature fluctuations ΔT should be appropriately described by a Gaussian distribution.

The recent release of the three-year high angular resolution and low instrument noise CMB measurements from the Wilkinson microwave anisotropy probe (WMAP) [1] offered the opportunity to analyse, with unprecedent precision, their temperature distribution in order to test the Gaussian hypothesis. These WMAP maps [2], with parameter resolution $N_{side} = 512$, divided the celestial sphere into $3,145,728$ equal sized areas, termed pixels, each one with an assigned highly precise ΔT value. Because measurements in the region around the Galactic Plane are strongly contaminated with foregrounds, they shall be eliminated from the data set in analysis by applying a cut-sky mask. The remaining ~ 2.5 million pixels guarantee a fine adjustment of the temperature distribution histogram (also termed *one-point distribution function*) to a smooth curve, thus minimizing the uncertainty of any (Gaussian or non-Gaussian) fitting.

Through the Minkowski functional's analysis, the WMAP team placed tight new limits on non-Gaussian temperature fluctuations in the CMB, thus concluding

that these data are consistent with Gaussianity [3,4]. However, several kinds of non-Gaussian features have been reported in the first-year and three-year WMAP data [5]. Clearly, the detailed study of the Gaussian random hypothesis must take into account the possibility that deviations from Gaussianity may have non-cosmological origins, such as unsubtracted foreground contamination, instrumental noise, and/or systematic effects [6]. Nonetheless, it is also possible that deviations from Gaussianity, although small, may be intrinsic to the CMB radiation [7] or have some other cosmological origin such as cosmic strings [8]. The related issue regarding the violation of the large-scale statistical isotropy, termed the North-South asymmetry, has also been extensively investigated in a variety of analyses, using different mathematical-statistical tools, with the first-year WMAP data [9] and more recently also with the three-year data [10].

Given the potential importance of these reported non-Gaussian features for our understanding of the physics of the early universe, all these analyses must be considered as non-exhaustive and further studies have to be performed. Although these non-Gaussian findings [7] —obtained with the first-year WMAP data— could be interpreted as unremoved foregrounds and/or instrumental noise, a comparative analysis with three-year data, where the signal-to-noise ratio increases due to a greater number of observations *per* pixel, could confirm or discard some of these possible explanations, or simply put better limits of their effect on the CMB data. This converts the analyses of the statistical properties of the WMAP three-year data into a necessary and important task.

Nonextensive statistical mechanics appears to be suitable to describe statistical properties of long-range correlated systems [11], like the primordial CMB radiation filling the universe. For such systems, correlations are expected to break down the Gaussian, *i.e.*, essentially uncorrelated, properties [12]. In that situation, the q-index can be seen as a scalar measure of the correlation range present in the system. For example, for an attractive two-body potential decaying as $1/r^\alpha$, $\alpha > 0$, in a d-dimensional classical system, we may expect q to increase above unity when α/d decreases below unity [13].

In what follows we perform a brief overview of the non-Gaussian distributions emerging from nonextensive statistical mechanics.

Basics of nonextensive statistical mechanics. – The probability distribution function P_q in the frame of the nonextensive statistical mechanics results [7] from the optimization of the q-entropy defined [14] (see [15] for various applications, and [16] for a new experimental confirmation) as follows ($q \in \Re$):

$$S_q \equiv k \, \frac{1 - \int \mathrm{d}x \, [P(x)]^q}{q-1},$$
$$S_1 = S_{BG} \equiv -k \int \mathrm{d}x \, P(x) \ln[P(x)], \qquad (1)$$

satisfying suitable constraints (*BG* stands for *Boltzmann-Gibbs*). Given two independent systems Σ_A, Σ_B (in the sense that $P_q^{\Sigma_A \cup \Sigma_B} = P_q^{\Sigma_A} P_q^{\Sigma_B}$), the pseudoadditivity property says that $S_q^{\Sigma_A \cup \Sigma_B} = S_q^{\Sigma_A} + S_q^{\Sigma_B} + (1-q)S_q^{\Sigma_A} \times S_q^{\Sigma_B}$. In other words, $(1-q)$ is a measure of the nonadditivity of the total system $\Sigma_A \cup \Sigma_B$. Clearly, the standard, extensive, statistical mechanics is recovered in the $q \to 1$ limit.

From eq. (1) one deduces [7] (see also [17] regarding the connection with the q-central limit theorem)

$$P_q(\Delta T) = A_q \, e_q^{-B_q(\Delta T)^2}, \qquad (2)$$

where in general B_q depends on the q-index, and A_q is the normalization constant obtained in such a way that $\int \mathrm{d}x \, P_q(x) = 1$. The q-exponential is defined by

$$e_q^z \equiv [1 + (1-q)z]^{1/(1-q)}, \quad \text{for } [1 + (1-q)z] \geqslant 0, \qquad (3)$$

and $e_q^z = 0$ otherwise. In the limit $q \to 1$, we recover the Gaussian distribution

$$P_q(\Delta T) \to P_1 \equiv P^{\mathrm{Gauss}}(\Delta T) = A \, e^{-B(\nu)(\Delta T)^2}, \qquad (4)$$

where $A \equiv 1/(\sigma_\nu \sqrt{2\pi})$, $B(\nu) \equiv 1/(2\,\sigma_\nu^2)$, and σ_ν^2 is the variance of the Gaussian distribution.

We shall use the nonextensive probability distribution P_q, defined in eqs. (2) and (3), to study the CMB temperature distribution P^{CMB} from the WMAP three-year data. Notice that by plotting the temperature distribution histogram in the form of the number of pixels *vs.* $(\Delta T/\sigma_\nu)^2$ any Gaussian distribution fits a straight line, thus recognizing departures from Gaussianity (*i.e.*, from linearity) becomes easy. For a clear comparison between the Gaussian (linear) and the nonextensive distributions we shall plot both distributions P_q and P^{Gauss} having equal value at the initial point $\Delta T = 0$ (that is, $A_q = A = 1$). Moreover, we observe that the best-fitting tangent line at that point has equal slope for both distributions, which implies that $B_q = B(\nu)$ (this procedure is consistent with the fact that $\mathrm{d}e_q^z/\mathrm{d}z|_{z=0} = 1, \forall q$). Therefore, the best-fitting of the CMB data through the nonextensive distributions is obtained by adjusting only the q-index.

WMAP data analyses. – We analyse the WMAP three-year data by exploring their temperature distribution in terms of Gaussian and nonextensive probability distributions. Since any non-Gaussian signature is revealed as non-linearities when the temperature distributions are plotted in the form of the number of pixels *vs.* $(\Delta T/\sigma_\nu)^2$, we present our results using this type of plots. We use the χ^2/degree of freedom (dof) estimator test to fit the data with the best Gaussian and nonextensive distributions functions.

We investigate these data corresponding to the Q, V, and W bands (central frequencies at 40.7, 60.8, and 93.5 GHz, respectively) by analysing the eight foreground reduced differencing assemblies (DAs) available at [2],

Table 1: All the variances are in units: $\times 10^3 \mu \mathrm{K}^2$. Analyses of the 8 DA CMB maps, $N_{\mathrm{Kp0}} = 2,407,737$ pixels. DE means "direct evaluation" from the corresponding CMB map. According to the χ^2 best-fit estimator, the temperature distributions of these CMB data are described by P_q distributions with variance σ_ν^2 and q-index: $q = 1.04 \pm 0.01$.

DA map	$\sum(1/n_i)$	σ_0^2	$\sigma_{\mathrm{noise}}^2$	σ_ν^2	$\sigma_{\mathrm{CMB}}^2 = \sigma_\nu^2 - \sigma_{\mathrm{noise}}^2$	$\sigma_{\nu\text{-DE}}^2$	$\sigma_{\mathrm{CMB\text{-}DE}}^2 = \sigma_{\nu\text{-DE}}^2 - \sigma_{\mathrm{noise}}^2$
$Q1$	4925.6	5039.58	10.31	16.03	5.7	17.02	6.7
$Q2$	4921.9	4556.94	9.32	14.93	5.6	15.94	6.6
$V1$	3655.2	10916.4	16.57	22.94	6.4	23.93	7.4
$V2$	3655.3	8677.74	13.17	19.46	6.3	20.60	7.4
$W1$	2437.1	34613.2	35.04	40.32	5.3	42.81	7.8
$W2$	2444.8	42672.3	43.33	48.08	4.8	50.72	7.4
$W3$	2445.0	47401.8	48.14	52.63	4.5	55.53	7.4
$W4$	2430.4	45482.9	45.91	50.51	4.6	53.71	7.8

namely $Q1$, $Q2$, $V1$, $V2$, $W1$, $W2$, $W3$, and $W4$. These DA CMB maps were corrected by the WMAP team for the galactic foregrounds (free-free, synchrotron, and dust emission) using the 3-band, 5-parameter template fitting method described in [1]. However, the foreground removal is only applicable to regions outside the Kp2 mask (which cuts $\sim 15\%$ of the sky data). The more severe cut, represented by the Kp0 mask (which excludes $\sim 23\%$ of the sky data), is recommended [1] for the statistical analysis of the CMB maps. Thus, for our analyses we have used the Kp0 mask. For the sake of completeness, we have also examined the foreground-reduced coadded maps Q $(= Q1 \oplus Q2)$, V $(= V1 \oplus V2)$, and W $(= W1 \oplus W2 \oplus W3 \oplus W4)$, as well as the coadded $V \oplus W$ map, formed by the six DAs $V1 \oplus V2 \oplus W1 \oplus W2 \oplus W3 \oplus W4$, and the coadded $Q \oplus V \oplus W$ map, formed by the eight DAs (the $\oplus$ symbol means the coadded sum of CMB maps as defined in [18]).

Finally, we also investigated the temperature distribution in the four quadrants of the celestial sphere (NE, NW, SW, and SE) in order to test the claimed large-scale anomaly [9,10] in the CMB temperature fluctuations data.

As pointed out in [8], the signal measured at any pixel in the microwave sky is made of several components $T_{\mathrm{pixel}} = T_{\mathrm{foregrounds}} + T_{\mathrm{noise}} + T_{\mathrm{CMB}}$, corresponding to foreground contamination signals, the noise from the instruments, and the CMB temperature fluctuations, respectively. Foreground contributions are expected around the galactic plane and from point sources. Given the fact that the instrument noise in the map is inhomogeneous (higher in the ecliptic plane than near the poles), the contribution from T_{noise} is important. For the subtraction of the foregrounds from CMB maps we used, as mentioned above, the most severe cut-sky, i.e., the Kp0 mask (for comparison, we also made the analyses with the Kp2 mask). The masks are provided by the WMAP team [1] and allow for the selective exclusion of portions of the sky basically due to contaminating radiative processes from our galaxy, including a 0.6 degree radius exclusion area around known point sources in the celestial sphere. The application of a mask to a CMB map simply means that, for a given pixel, a mask value of zero implies that it is excluded; a value

of one means that it is accepted. Moreover, since the galactic foregrounds contribute as positive temperature contaminations, we perform the analyses of the one-point distributions considering only the negative temperature fluctuations data. In this way, the first term in the above equation is dropped and one is left with CMB signal plus the signal from the instrument noise (the signal noise is Gaussian per observation [8,18]). What converts the instrument noise in a non-Gaussian signal is the non-uniform way in which the CMB sky was observed, because some regions were largely more observed than others, making such a noise to be different from pixel to pixel. The way out to deal with this problem is to characterize its shape and intensity through Monte Carlo realizations of similar sky data observations.

Consider the remaining effects by defining [8] the variance of the total signal T_{pixel} as

$$\sigma_\nu^2 \equiv \sigma_{\mathrm{pixel}}^2 = \frac{\sigma_0^2}{n_i} + \sigma_{\mathrm{CMB}}^2 \,, \qquad (5)$$

where n_i is the number of observations for the i-th pixel, σ_0^2 is the noise variance per observation of a given instrument [1], and σ_{CMB}^2 is the variance of the CMB temperature fluctuations. The mean contribution of the instrumental noise can be estimated by considering the effect of the different number of observations for each pixel. This can be done with the effective variance due to the non-stationary instrument noise [8]

$$\sigma_{\mathrm{noise}}^2(\nu) = \frac{\sigma_0^2 \sum_{i=1}^N (1/n_i)}{N} \,, \qquad (6)$$

where N is the total number of pixels considered in the analysis of the map. The values of $\sum(1/n_i)$ for each WMAP DA map are given in table 1 (Kp0 mask case). The total number of pixels N with CMB signal corrected for galactic contaminations results from the application of the cut-sky mask, that is $N = N_{\mathrm{Kp0}} = 2,407,737$ for the Kp0 mask, or $N = N_{\mathrm{Kp2}} = 2,664,479$ for the Kp2 mask. Thus, the effective noise variances $\sigma_{\mathrm{noise}}^2(\nu)$ and the variances σ_ν^2 leads to the CMB variance

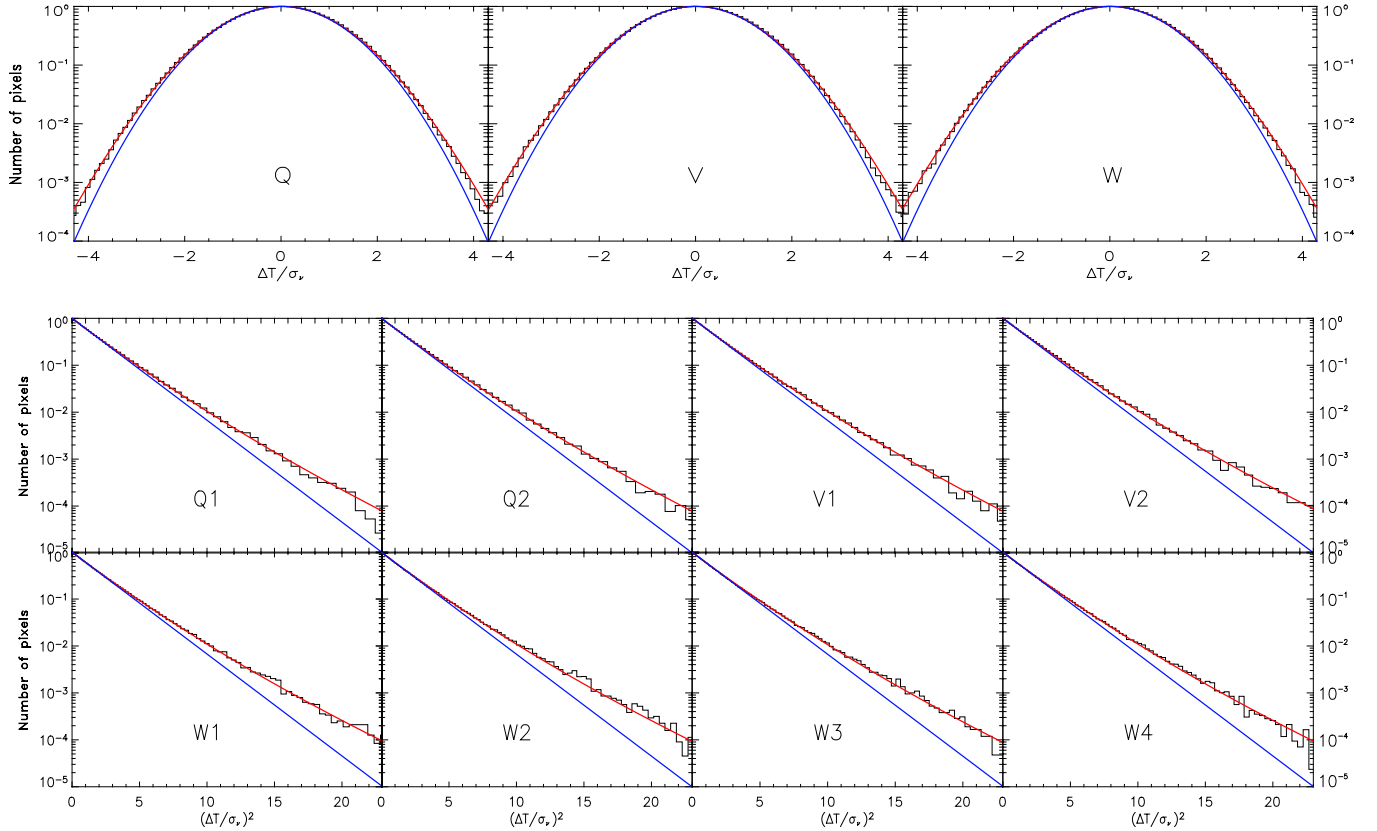$$\sigma_{\mathrm{CMB}}^2 = \sigma_\nu^2 - \sigma_{\mathrm{noise}}^2(\nu) \,. \qquad (7)$$

Fig. 1: (Colour on-line) Top: fits to the (positive and negative) WMAP CMB temperature fluctuations data, corresponding to the Q, V, and W coadded maps (after the Kp0 cut-sky), in the number of pixels *vs.* $\Delta T/\sigma_\nu$ plots. We show the χ^2 best-fits: Gaussian distribution (blue curve) with $\sigma_Q = 104\,\mu$K, $\sigma_v = 118\,\mu$K, and $\sigma_W = 131\,\mu$K, respectively, and each nonextensive distribution (red curve) P_q with $q = 1.04$. Bottom: similar analysis, but now with the eight DA WMAP maps ($Q1,\ldots,W4$) after applying the Kp0 mask. We plotted the number of pixels *vs.* $(\Delta T/\sigma_\nu)^2$ to enhance the non-Gaussian behavior. To avoid possible unremoved galactic foregrounds, we consider only the negative temperature fluctuations. Again, we show the χ^2 best-fits: Gaussian distribution (blue curve) and nonextensive distribution (red curve) P_q, now with $q = 1.04 \pm 0.01$.

Although both σ_ν^2 and $\sigma_{\rm noise}^2(\nu)$ depend on the map under analysis, their difference is independent of the map. In other words, if the treatment of instrumental noise is correct, the CMB variance $\sigma_{\rm CMB}^2$ should be the same for the maps under investigation (Q, V, and W).

The present best-fit data analyses were obtained according to the χ^2/degree of freedom (dof) estimator test. Thus, the typical $\chi^2/200$ values for the Gaussian fits are 2×10^{-2}, and the $\chi^2/200$ values for the nonextensive temperature distribution are 2×10^{-3}. Analyses performed using 300 dof and 400 dof, instead of 200 dof, result in similar best-fitting values. In addition, we have not detected any significant difference using the Kp2 mask instead of the Kp0 mask.

Our analyses of the eight DAs is as follows. Once the variances σ_ν^2 have been determined through the χ^2 best-fit Gaussian temperature distribution (blue on-line lines in fig. 1), we use the effective noise variance $\sigma_{\rm noise}^2$, given in eq. (6), to calculate the CMB variances $\sigma_{\rm CMB}^2$ (see table 1). This approach validates, although *a posteriori*, the use of the effective noise variance as representing the mean contribution of the instrumental noise and our previous

results. The CMB variances we obtain for the Q, V and W coadded maps are $\sigma_{\rm CMB}^2 = 5.98$, 6.56, $6.77 \times 10^3 \mu$K^2, respectively.

Summarizing, the temperature distribution analyses of the coadded Q, V, and W CMB maps, as well as the eight individual DAs maps shown in fig. 1, exhibit that the distribution of the CMB temperature fluctuations does not obey a Gaussian distribution. The analysis of the other coadded CMB maps, mentioned before, produces a result that is fully consistent with this one.

Another way to test Gaussianity in a given data set is the calculation of the factor involving the 4th- and 2nd-momenta of the distribution, $R \equiv \langle \Delta T^4 \rangle / \langle 3\Delta T^2 \rangle^2$, where $\langle x^n \rangle \equiv \int {\rm d}x\, P(x)\, x^n$ ($R = 1$ corresponds to the Gaussian distribution case). All the CMB maps analysed results in $R \in [1.02, 1.06]$, which validates the possible description, within the four available ordinate decades, of the WMAP data using the P_q distributions emerging from nonextensive statistical mechanics.

We also studied the coadded W map, after applying the Kp0 mask, in the four quadrants: North-East (NE), North-West (NW), South-West (SW), and South-East (SE) of

the celestial sphere. It turns out that the temperature distribution of the CMB data is sensibly different in one of these four sky patches. Indeed, we found $q_{NE} \simeq 1.015$, $q_{NW} \simeq 1.01$, $q_{SW} \simeq 1.02$, and $q_{SE} \simeq 1.05$, with $R = 1.02, 1.01, 1.025$, and 1.04, respectively.

The significance of the q-index values found are based on the robustness of our findings. In fact, all our results are the same independently of the frequency-map or the coadded-map analysed. Also, they are equal for the two cut-sky masks applied, and for the one-year [7] and three-year maps.

Monte Carlo analysis. – Now we present the results of our analyses considering the WMAP Monte Carlo (MC) simulations, which contain the instrument noise having a spatially varying noise structure, like real data.

As a matter of fact, the WMAP detectors noises are inhomogeneous. This is due to the fact that the regions around the ecliptic poles (NW and SE quadrants) have large number of observations (N_{obs}), and therefore low statistical noise, while the region corresponding to the ecliptic plane (NE and SW quadrants) were less observed (lower N_{obs} values), and have large statistical noise. The spatially varying noise structure for each DA CMB map, with simulated instrument noise that include all known radiometric effects, were properly realized by the WMAP team in a set of MC sky realizations for each DA (available at http://lambda.gsfc.nasa.gov/product/map/dr1/noise_sims_imaps.cfm). These MC data constitute an important tool for instrument noise evaluation corresponding to each DA, and also for the MC-coadded maps, obtainable for each one of the three bands (Q, V, and W) by combining MCs from different DAs. For instance, to obtain a MC-coadded CMB map in the Q band, one chooses $Q1^i$ from the set of MCs for the DA-$Q1$, and combine (in a coadded way, according to [18]) with $Q2^j$ from the set of MCs for the DA-$Q2$.

This time, the noise instrument of a given map is treated by computing the variance-normalized temperature for each pixel (a procedure described in [19]: see, in particular, eq. (17)). We observe that the instrument noise shows non-Gaussian behavior whose strength and signature are different to what is observed in our analyses of the 3-year WMAP data. In average, we obtained χ^2 best-fits with distributions P_q with $q = 1.1 \pm 0.02$, and after the variance-normalization, the q-index maintain its value, although the variance is clearly modified.

Moreover, we noticed that the non-Gaussian features of the instrument noise are sensible to N_{obs}, in the sense that the q-index of the P_q distributions changes significantly when analysing two regions in the sky, namely, one that was observed (at least) twice the other. This interesting (and expected) feature is absent in the three-year WMAP data when compared with the (less observed) one-year WMAP data [7]; in fact we obtained essentially the same q-index for both data sets. Finally, we have also to mention that such strong non-Gaussianities, present in all the coadded-MCs, exhibit a high symmetry between the SE and NW quadrants: $q_{SE}/q_{NW} = 1.0 \pm 10^{-3}$. Again, this feature is fully absent in WMAP data, where we have $q_{SE}/q_{NW} \simeq 1.04$.

Comments and conclusions. – Some comments are due regarding the use of DA maps and the application of two WMAP masks, Kp0 and Kp2, in our analysis. First, we analysed frequency by frequency (Q, V and W bands) because the CMB galactic foregrounds (free-free, synchrotron, and dust emission) are frequency dependent, which means that, if they are still present in the WMAP data, they should manifest differently at each frequency. Moreover, as recommended by the WMAP team, we have analysed the foreground reduced CMB maps [2], which were produced using the foreground template model to subtract the synchrotron, free-free, and dust emission from the measured sky maps [1]. Our analyses of the one-point distributions of all these WMAP CMB maps do not show significant differences in the value of the q-index for the data investigated. Second, another way to examine the possible presence of unremoved foregrounds is by analysing the CMB data using different cut-sky masks. We performed such analyses using both the Kp0 and Kp2 masks and, according to the χ^2 best-fit estimator, we do not found significant difference in the values of the q-index. Third, known galactic foregrounds contribute with positive temperature fluctuations contaminations. Hence, we consider only the negative temperature fluctuations of the CMB maps to perform our data analyses (see the bottom plots of fig. 1). These procedures, and their corresponding results, show that possible unremoved galactic foregrounds could not be responsible for the detected non-Gaussian signatures.

Now consider the instrument noise, which is always convolved with the CMB signal. In WMAP maps the instrument noise is inhomogeneous, higher in the ecliptic plane (roughly NE and SW quadrants) than near the ecliptic poles (NW and SE quadrants), and their contribution to T_{pixel} may cause a non-Gaussian behavior, as one can observe in MC sky maps simulated by the WMAP team. However, two interesting facts make the non-Gaussian noise signals qualitative and quantitatively different from what is observed in WMAP data. We emphasize that, in order to deal with inhomogeneous instrument noise in our CMB analyses, we have taken into account the following two procedures: the coadded sum of CMB DAs maps, as described in [18], and the variance-normalized temperature, as described in [19]. First, the instrument noise is extremely sensible to N_{obs}, as expected, and as MC simulations confirm. It is well known that sky pixels in three-year WMAP data have been observed roughly 3 times more than one-year data, nevertheless the P_q distributions are the best-fit one-point distributions, with $q = 1.04 \pm 0.01$, for both data sets (see [7]). Second, the non-Gaussian signals from inhomogeneous instrument noise exibit a high symmetry between

the NW and SE quadrants that has been quantifiable using the MC maps: $q_{\mathrm{SE}}/q_{\mathrm{NW}} = 1.0 \pm 10^{-3}$; nonetheless this feature is fully absent in WMAP data, where we have $q_{\mathrm{SE}}/q_{\mathrm{NW}} \simeq 1.04$. These two facts strongly indicate that any subtle effect coming from inhomogeneous instrument noise contamination could not explain the presence of non-Gaussian signatures in the analysed WMAP data.

Summarizing, we have shown that a Gaussian distribution is excluded, at the 99% CL, to properly represent the overall CMB temperature fluctuations measured by WMAP. Through the temperature distribution analyses we notice that the three-year WMAP data are suitably explained, along about four decades, by a P_q distribution with $q = 1.04 \pm 0.01$. Moreover, our results also evidence that the strongest non-Gaussian contribution comes from the South-East quadrant, where $q_{\mathrm{SE}} \simeq 1.05$. Therefore, the hypothesis of a nonextensive nature for the CMB temperature fluctuations is quite plausible.

$$* * *$$

REFERENCES

[1] Hinshaw G. *et al.*, astro-ph/0603451; Jarosik N. *et al.*, astro-ph/0603452.

[2] http://lambda.gsfc.nasa.gov/product/map/dr2/maps_da_r9_iqu_fg_3yr_get.cfm; http://lambda.gsfc.nasa.gov/product/map/dr2/maps_band_r9_iqu_fg_3yr_get.cfm.

[3] Komatsu E. *et al.*, *Astrophys. J. Suppl.*, **148** (2003) 119.

[4] Eriksen H. K. *et al.*, *Astrophys. J.*, **612** (2004) 64; Hansen F. K. *et al.*, *Astrophys. J.*, **607** (2004) L67; Creminelli P. *et al.*, *J. Cosmol. Astropart. Phys.*, **0605** (2006) 004.

[5] Chiang L.-Y. *et al.*, *Astrophys. J.*, **590** (2003) L65; Vielva P. *et al.*, *Astrophys. J.*, **609** (2004) 22; Park C.-G., *Mon. Not. R. Astron. Soc.*, **349** (2004) 313; Larson D. L. and Wandelt B. D., *Astrophys. J.*, **613** (2004) L85; Naselsky P. D. *et al.*, *Astrophys. J.*, **615** (2004) 45; Cayon L., Jin J. and Treaster A., *Mon. Not. R. Astron. Soc.*, **362** (2005) 826; Liguori M. *et al.*, astro-ph/0509098; McEwen J. D. *et al.*, astro-ph/0604305; Cruz M. *et al.*, astro-ph/0603859.

[6] Eriksen H. K. *et al.*, *Astrophys. J.*, **622** (2005) 58; Wibig T. and Wolfendale A. W., *Mon. Not. R. Astron. Soc.*,

[7] Bernui A., Tsallis C. and Villela T., *Phys. Lett. A*, **356** (2006) 426.

[8] Jeong E. and Smoot G. F., *Astrophys. J.*, **624** (2005) 21.

[9] Eriksen H. K. *et al.*, *Astrophys. J.*, **605** (2004) 14; de Oliveira-Costa A. *et al.*, *Phys. Rev. D*, **69** (2004) 063516; Hansen F. K., Banday A. J. and Gorski K. M., astro-ph/0404206; Copi C. J. *et al.*, astro-ph/0508047; Bernui A. *et al.*, *Astron. Astrophys.*, **464** (2007) 479; Bernui A. *et al.*, *Astron. Astrophys.*, **454** (2006) 409.

[10] Copi C. J. *et al.*, astro-ph/0605135; de Oliveira-Costa A. and Tegmark M., astro-ph/0603369; Wiaux Y. *et al.*, *Phys. Rev. Lett.*, **96** (2006) 151303; Abramo L. R. *et al.*, *Phys. Rev. D*, **74** (2006) 063506; Ghosh T., Hajian A. and Souradeep T., astro-ph/0604279; Helling R. C. *et al.*, astro-ph/0603594; Adler R. J., Bjorken J. D. and Overduin J. M., gr-qc/0602102; Cresswell J. G. *et al.*, *Phys. Rev. D*, **73** (2006) 041302; Vielva P. *et al.*, astro-ph/0609147.

[11] Caruso F. and Tsallis C., cond-mat/0612032.

[12] Hamity V. H. and Barraco D. E., *Phys. Rev. Lett.*, **76** (1996) 4664; de Oliveira H. P., Sautu S. L., Soares I. D. and Tonini E. V., *Phys. Rev. D*, **60** (1999) 121301; de Oliveira H. P., Soares I. D. and Tonini E. V., *Phys. Rev. D*, **67** (2003) 063506.

[13] Rapisarda A. and Pluchino A., *Europhys. News*, **36** (6) (2005) 202.

[14] Tsallis C., *J. Stat. Phys.*, **52** (1988) 479.

[15] Gell-Mann M. and Tsallis C. (Editors), *Nonextensive Entropy – Interdisciplinary Applications* (Oxford University Press, New York) 2004; Boon J. P. and Tsallis C. (Editors), *Nonextensive Statistical Mechanics: New Trends, New Perspectives*, Vol. **36** (European Physical Society) 2005, p. 6; Tsallis C., Gell-Mann M. and Sato Y., *Proc. Natl. Acad. Sci. U.S.A.*, **102** (2005) 15377; Tsallis C., Anjos J. C. and Borges E. P., *Phys. Lett. A*, **310** (2003) 372; Lyra M. L. and Tsallis C., *Phys. Rev. Lett.*, **80** (1998) 53; Beck C., *Phys. Rev. Lett.*, **87** (2001) 180601; Borges E. P. *et al.*, *Phys. Rev. Lett.*, **89** (2002) 254103.

[16] Douglas P., Bergamini S. and Renzoni F., *Phys. Rev. Lett.*, **96** (2006) 110601.

[17] Moyano L. G., Tsallis C. and Gell-Mann M., *Europhys. Lett.*, **73** (2006) 813; Umarov S., Tsallis C. and Steinberg S., cond-mat/0603593; Umarov S., Tsallis C., Gell-Mann M. and Steinberg S., cond-mat/0606038; cond-mat/0606040.

[18] Jarosik N. *et al.*, *Astrophys. J. Suppl.*, **148** (2003) 29.

[19] Spergel D. N. *et al.*, astro-ph/0603449.

[20] Górski K. M. *et al.*, *Astrophys. J.*, **622** (2005) 759, http://healpix.jpl.nasa.gov/.